J. Fluid Mech. (1991), *vol.* 229, *pp.* 205–228
Printed in Great Britain

Thermocapillary stabilization of the capillary breakup of an annular film of liquid

By HENK A. DIJKSTRA† AND PAUL H. STEEN
Mathematical Sciences Institute and School of Chemical Engineering, Cornell University, Ithaca, NY 14853, USA

(Received 24 August 1989 and in revised form 11 January 1991)

It is known that the breakup by surface tension of a cylindrical interface containing a viscous liquid can be damped by axial motion of the underlying liquid and that for an annular film the capillary instability can be completely suppressed (disturbances of all wavelengths decay) by certain axial velocity profiles. Here, using a linear stability analysis, it is shown that complete stabilization can also occur for thermocapillary-driven axial motions. However, the influence of thermocapillary instabilities typically shrinks the window in parameter space where stabilization is found, relative to the isothermal case. The influence of Reynolds, surface tension, Prandtl, and Biot parameters on limits of stabilization is calculated using continuation techniques. It is observed that windows of stabilization first open with topological changes of the neutral curves in parameter space. A long-wave analysis unfolds the nature of the singularities responsible for several of these topological changes. The analysis also leads to the physical mechanism responsible for (long-wave) stabilization and in certain cases to necessary conditions for (long-wave) stabilization.

1. Introduction

The capillary instability of a cylindrical interface can be dramatically influenced by the velocity profile of the liquid it contains (Xu & Davis 1985; Russo & Steen 1989). Base states with certain axial motions are found to be stable to disturbances of all wavelengths according to linear theory (Russo & Steen 1989). However, the axial motions for which complete stabilization has been found so far have been generated by mechanical means, *viz.* applied interfacial shear and applied axial pressure gradients (i.e. isothermally). We ask whether axial motions driven by thermocapillary forces will also give complete stabilization; i.e. will the coupling of the thermal and mechanical disturbances destroy the stabilization observed in the isothermal case?

Complete stabilization opens intriguing possibilities for technological application. Indeed, the effect has already been exploited to a limited extent in order to transport heavy crude through pipelines more efficiently by using a less viscous liquid to lubricate the pipe wall. A stable interface between the oil-core and the lubricant-annulus is the key to reducing the required pumping power (Charles, Govier & Hodgson 1961; Russel & Charles 1959; Zubillaga *et al.* 1985). It has been shown more recently (e.g. Preziosi, Chen & Joseph 1989) that this core–annular flow (in the absence of gravity) can be completely stable for certain viscosity ratios. Other

† Current address: Institute of Meteorology and Oceanography, University of Utrecht, The Netherlands.

(potential) applications include processes for producing materials which depend on interfacial tension to contain a melt. Examples of such processes are liquid-encapsulated Czochralski crystal growth, float-zone crystal growth under low-gravity conditions, and the 'Taylor-wire' process for the manufacture of metallic wires. Furthermore, thermocapillary stabilization may explain the apparent observation of a very long stable interface (nearly twice the static limit) in a molten indium sample taken from a float-zone experiment in a space laboratory (STS Flight 41D, September 1984, Murphy *et al.* 1987).

Xu & Davis (1985) consider a liquid cylinder in a gas and consider both thermocapillary- and mechanically-driven applied shear. In both cases the capillary breakup is suppressed, but not completely. Russo & Steen (1989) consider a broader class of geometry, a liquid bridge of annular cross-section, but restrict to the isothermal case. The bridge is bounded on the inside by a rigid rod. They find that complete stabilization is favoured by small gap ratios (the ratio of the depth of the liquid layer to the mean interface radius); however, stabilization can occur for gap ratios up to about $\frac{1}{2}$ for the most favourable base flow.

Here, base flows where the shear is caused by a gradient in surface tension induced by a linear temperature gradient along the interface are considered. Hydrothermal (thermocapillary) instabilities compete with the capillary instability and both are influenced by the base flow. We find that although thermal effects do not completely destroy the isothermal stabilization they do weaken it.

First we consider a one-parameter family of base states, parametrized by the strength of the thermocapillary force and subject to a constant ambient pressure field. The study of the linear stability of these base states shows that for small layer thicknesses, there exists a range of Reynolds numbers (driving force due to applied shear stresses generated by thermocapillarity), moderate but not too large, for which disturbances are completely stabilized. Stabilization is favoured at small Prandtl number P, relatively small surface tension number S and large Biot number B. For large P and large S, complete stabilization is not possible.

Next, we generalize to a two-parameter family of base states where the new parameter is the axial pressure gradient. Although members of this family may be difficult to realize in experiment, their consideration leads to a clearer understanding of the physics. The stability behaviour of these base states is qualitatively like that of the isothermal case where a similar parametrization is used. Complete stabilization disappears for base states with a slight 'return flow' character; these states become unstable to long waves. The range of Reynolds numbers corresponding to stabilization and the influence of the other parameters on this range is reported.

The numerical solution of the linear stability equations for all wavelengths suggests that the heart of the physics responsible for complete stabilization can be captured with a long-wave analysis. Indeed, long-wave asymptotics reveal the structure of singularities in the 'neutral surfaces' of the parameter space which characterize the 'birth' of stabilization. Furthermore, this analysis shows that the physical mechanism for stabilization, which in the isothermal case depends on a (laminar) Reynolds stress interaction with the base flow, is modified by the thermal field but in a way which leaves its essential features unchanged.

The main contributions of this paper are the description of the mechanism of stabilization, and the analysis of the singularities in the neutral curves in the long-wave limit; each is the first of its kind as far as we are aware. The numerical computations are more important as they relate to and frame the long-wave analysis perhaps than for the results in themselves. Indeed, these results are anticipated to a

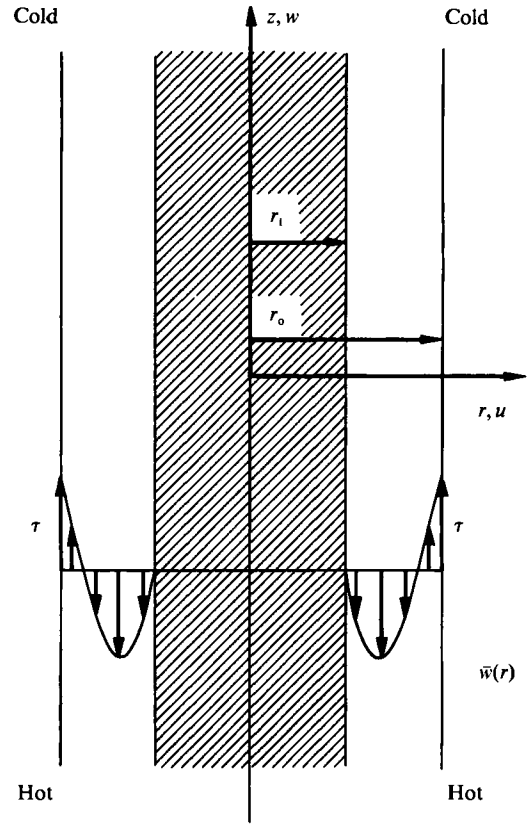

FIGURE 1. Sketch of the annular liquid bridge. The shaded area is the rigid rod, the equilibrium interface is at $r = r_0$. The shear stress τ for the thermocapillary base state is caused by a linear temperature difference along the interface.

certain extent by the isothermal analysis (Russo & Steen 1989). Furthermore, the long-wave analysis is useful as a relatively easy and inexpensive guide to interesting regions in parameter space where a full numerical analysis can then supply details.

2. Formulation

Consider an infinitely long axisymmetric liquid bridge of annular cross-section bounded laterally on the inside by a rigid rod with radius r_i and on the outside by a gas–liquid interface of mean radius r_0 (figure 1). The bridge is composed of an incompressible Newtonian liquid having dynamic viscosity μ, density ρ and mean surface tension σ_0, i.e. at temperature T_0^*. The thermal diffusivity of the liquid is k. Let $H = r_0 - r_i$ denote the mean depth of the liquid layer.

A constant temperature gradient $dT^*/dz^* = -b$, $b > 0$, is imposed along the axis of the bridge. The surface tension σ is assumed to depend linearly on the interfacial temperature T^*, i.e. $\sigma = \sigma_0(1-\zeta(T^*-T_0^*))$, where T_0^* is the interface temperature, say at $z^* = 0$. The temperature gradient induces a shear stress $\tau = \sigma_0 \zeta b$ at the interface. Gravity is assumed absent. A dimensionless temperature T is defined by $T^* - T_0^* = bHT$.

Following Xu & Davis (1985) and Russo & Steen (1989), velocity, length, time and pressure are scaled with $W_c = (\sigma_0/\rho H)^{\frac{1}{2}}$, H, H/W_c and σ_0/H, respectively. In addition,

a second velocity scale associated with the shear stress at the interface due to thermocapillarity, $W_b = \tau H/\mu$, is identified.

A cylindrical coordinate system (r, ϑ, z) is used. Let the interface be described as $r = \eta(\vartheta, z)$ and let the velocity vector $\boldsymbol{q}$ have components (u, v, w). In non-dimensional variables, the equations describing the evolution of the flow in the bridge and the interface are presented in Xu & Davis (1985).

The heat flux balance at the interface is given by the equation

$$-\left[1+\frac{\eta_\vartheta^2}{r^2}+\eta_z^2\right]^{-\frac{1}{2}}\left[T_r-\frac{\eta_\vartheta T_\vartheta}{r^2}-\eta_z T_z\right] = B(T-T_a)+Q, \tag{1}$$

where Q is a heat flux imposed on the surrounding environment (determined by the base state under consideration) and T_a is the temperature of the ambient gas far from the interface. Various choices of Q have been used in the literature and below we keep two choices in order to compare with previous work.

The dimensionless groups in the equations are the Biot number B, the surface tension number S, the Reynolds number R, the Prandtl number P and the ratio of the liquid layer depth to mean interfacial radius A,

$$B = \frac{hH}{k}, \quad S = \frac{\rho H \sigma_0}{\mu^2}, \quad R = \frac{\rho \tau H^2}{\mu^2}, \quad P = \frac{\mu}{\rho k}, \quad A = \frac{H}{r_0}, \tag{2}$$

where h is the surface heat transfer coefficient.

The boundary conditions at the (insulated) rigid wall $r = r_1/H$ are

$$u = v = w = 0, \; T_r = 0. \tag{3}$$

3. Base states

The base-state interface is perfectly cylindrical ($\bar{\eta} = A^{-1}$). Overbars denote quantities associated with the base-state solution. The induced shear stress at the interface drives a steady parallel shear flow in the bridge; let $\beta = (1-A)/A$ and $\gamma = 1/A$ denote the inner and outer boundaries of the radial domain, respectively. The solution for the velocity and pressure is given by

$$\bar{u} = \bar{v} = 0, \tag{4a}$$

$$\bar{w}(r) = \xi_1(r^2-\beta^2)+\xi_2 \ln\frac{r}{\beta}, \tag{4b}$$

$$\bar{p}_z = \delta, \tag{4c}$$

where

$$\xi_1 = \tfrac{1}{4}\delta S^{\frac{1}{2}}, \quad \xi_2 = S^{\frac{1}{2}}(R/(SA)-\delta/(2A^2)) \tag{4d,e}$$

and here δ is a constant. For a fixed geometry (fixed A), the axial velocity $\bar{w}(r)$ is a two-parameter family of profiles (parametrized by, say, ξ_1 and ξ_2). For a fixed uniform ambient pressure, the two parameters are related through the balance of normal stress at the interface, leaving a one-parameter family. This is one class of base states which we study below. However, it is useful to also consider the full two-parameter family of velocity profiles. To achieve these in the laboratory, one must arrange the ambient pressure to vary linearly in the axial direction with a gradient which depends on the parameters.

In order to make these two classes of base states precise, we first write down the base-state temperature field. The solution for the temperature is given by

$$T_a(z) = -z, \quad \bar{T}(r,z) = -z + \tilde{T}(r), \tag{5a}$$

$$\tilde{T}(r) = C_1 + S^{\frac{1}{2}}P[C_2 \ln r + C_3 r^4 + C_4 r^2 + C_5 r^2 \ln(r/\beta)], \tag{5b}$$

where $C_2 = -\frac{1}{4}\beta^2(\xi_2 + \beta^2\xi_1)$, $C_3 = -\frac{1}{16}\xi_1$, $C_4 = -C_2/\beta^2$ and $C_5 = -\frac{1}{4}\xi_2$. Now one can choose C_1 such that $\tilde{T}(\gamma) = 0$ and satisfy (1) by arranging $Q = -\tilde{T}_r(\gamma)$, or one can just put $Q = 0$ and determine C_1 from (1). In the first case the base-state temperature does not depend on B (for later reference this base state is called $\mathscr{B}_0$) where in the second case it does (called $\mathscr{B}_1$). We include both cases for comparison with previous results although we later restrict attention to the $\mathscr{B}_1$ base state.

The normal stress balance at the interface, which depends on the temperature field through the variation of surface tension, is described by the equation

$$p - p_a = A(1 - S^{-1}R(-z + \tilde{T}(\gamma)), \tag{6a}$$

where p_a is the ambient pressure field. In a constant ambient pressure field ($p_a =$ const) the exact solution for the base state pressure is given by

$$\bar{p}(z) - \text{const} = S^{-1}RA[z - \tilde{T}(\gamma)] + A \tag{6b}$$

and hence the parameters ξ_1 and ξ_2 are related by $\delta = S^{-1}RA$. In view of (4), these axial velocity profiles constitute a one-parameter family, parametrized, say, by $S^{-\frac{1}{2}}R$. Under thermal conditions corresponding to $\mathscr{B}_0$, the planar linear flow base state of Smith & Davis (1983) is recovered from this class of base states as $A \to 0$ (with a straightforward rescaling).

The more general class of base states is motivated by taking the gradient of (6*a*) which leads to the ambient pressure field

$$p_a(z) = (\delta - S^{-1}RA)\, z, \tag{7a}$$

and the base state pressure field

$$\bar{p}(z) = \delta z + A - S^{-1}RA\tilde{T}(\gamma). \tag{7b}$$

Here, for a fixed geometry, the family of velocity profiles (4*a*, *b*) is controlled by the parameter $\delta S^{\frac{1}{2}}$ in addition to $S^{-\frac{1}{2}}R$.

Several limiting cases of this class of base states are noteworthy. First, for an isothermal situation, $\bar{T}(r,z) = T_a =$ constant and hence $\tilde{T}(\gamma) = 0$ (take $P = 0$ for thermal conditions $\mathscr{B}_1$). The shear stress τ which appears in the definition of R in (2) now corresponds to a shear stress applied by mechanical means (i.e. a primitive parameter). The two-parameter family of base states considered by Russo & Steen (1989) are recovered. Of course, these also require a linear ambient pressure field.

A different limit, the base state of circular cross-section with thermocapillary-driven axial flow used in Xu & Davis (1985), can also be recovered by letting $A \to 1$. This requires the shear at the centre line to vanish ($\xi_2 = 0$ in (4*e*)) and hence that $\delta = 2S^{-1}R$. This effective replacement of the no-slip condition (3) by a boundedness condition at the centreline is completed by adding a constant to the base-state velocity. This base state is also an exact solution if a linear ambient pressure field is imposed. Otherwise, for a uniform ambient field, it is approximate with an error on the order of $S^{-1}R$.

Note that core–annular flow, where the fluid in the annulus is driven by a linear pressure gradient, is one realization of an imposed linear ambient pressure field. However, the interactions between core and annulus in the presence of disturbances

(stability) are broader in scope than those we consider and hence core–annular flow is not a subcase of our analysis.

4. Linear stability analysis

Each dependent variable is expressed as the sum of the base state and some small disturbance (denoted by a prime)

$$(\boldsymbol{q}, p, \eta, T) = (\bar{\boldsymbol{q}}, \bar{p}, \bar{\eta}, \bar{T}) + (\boldsymbol{q}', p', \eta', T'), \tag{8a}$$

and a 'normal mode' analysis is pursued, i.e.

$$(\boldsymbol{q}', p', \eta', T')(r, \vartheta, z, t) = (\hat{\boldsymbol{q}}(r), \hat{p}(r), \hat{\eta}, \hat{T}(r)) \exp\{\mathrm{i}(\alpha z + m\vartheta - \omega t)\}. \tag{8b}$$

In carrying out this analysis formally, there arises a problem in separating the linearized normal stress condition in z. This is due to the influence of the variation of the surface tension on the normal stress at the interface.

Two ways to accommodate a separation of variables are mentioned in Smith & Davis (1983); each constrains the results. One can either neglect the above-mentioned influence (cf. $\chi = 0$ in (11d) below) or take it approximately into account (cf. $\chi = 1$ in (11d) below). Either case leads to a restriction on the axial wavenumber α which takes the form

$$\frac{2\pi}{(SR^{-1} - \tilde{T}(\gamma))} \ll \alpha. \tag{9}$$

Note that for the case $\mathscr{B}_0$, the value of $\tilde{T}(\gamma)$ vanishes and the restriction is that used in Xu & Davis (1985) and Smith & Davis (1983). In case $\mathscr{B}_1$, equation (9) is more restrictive since $\tilde{T}(\gamma) > 0$. It will turn out that for the parameter range in which we are interested (large S, bounded R, small A) the condition (9) will not limit the results in any significant way.

We ignore the restriction (9) for the moment to obtain the structure of neutral curves for all wavenumbers and to obtain asymptotic expressions for the long-wave behaviour (small α).

Upon substitution of (8b) in the linearized equations an eigenvalue problem is obtained. Here only temporal instabilities are investigated and therefore the eigenvalue is $\omega = \lambda + \mathrm{i}\nu$. The real part λ is the angular frequency and the complex part ν is the growth rate. If $\nu > 0$ the base state is unstable, while if $\nu < 0$ it is linearly stable. The two-point eigenvalue problem for $(\hat{\boldsymbol{q}}, \hat{p}, \hat{\eta}, \hat{T})$, where $\hat{\boldsymbol{q}} = (\hat{u}, \hat{v}, \hat{w})$, is given by

$$u_r + \frac{1}{r}u + \frac{\mathrm{i}mv}{r} + \mathrm{i}\alpha w = 0, \tag{10a}$$

$$S^{-\frac{1}{2}}\left[u_{rr} + \frac{1}{r}u_r - u\left(\frac{m^2+1}{r^2} + \alpha^2\right) - \frac{2\mathrm{i}mv}{r^2}\right] - p_r = u(\mathrm{i}\alpha\bar{w} - \mathrm{i}\omega), \tag{10b}$$

$$S^{-\frac{1}{2}}\left[v_{rr} + \frac{1}{r}v_r - v\left(\frac{m^2+1}{r^2} + \alpha^2\right) + \frac{2\mathrm{i}mu}{r^2}\right] - \frac{\mathrm{i}mp}{r} = v(\mathrm{i}\alpha\bar{w} - \mathrm{i}\omega), \tag{10c}$$

$$S^{-\frac{1}{2}}\left[w_{rr} + \frac{1}{r}w_r - w\left(\frac{m^2}{r^2} + \alpha^2\right)\right] - u\bar{w}' - \mathrm{i}\alpha p = w(\mathrm{i}\alpha\bar{w} - \mathrm{i}\omega), \tag{10d}$$

$$S^{-\frac{1}{2}}\left[T_{rr} + \frac{1}{r}T_r - T\left(\frac{m^2}{r^2} + \alpha^2\right)\right] = P[T(\mathrm{i}\alpha\bar{w} - \mathrm{i}\omega) - w + u\tilde{T}'], \tag{10e}$$

where the hats are dropped for convenience and the primes denote derivatives in r. At $r = \gamma$,

$$u + \mathrm{i}\omega\eta - \mathrm{i}\alpha\eta\bar{w} = 0, \tag{11a}$$

$$v_r + A(\mathrm{i}mu - v + \mathrm{i}mS^{-\frac{1}{2}}R(\eta\tilde{T}' + T)) = 0, \tag{11b}$$

$$w_r + \eta\bar{w}'' + \mathrm{i}\alpha(u + S^{-\frac{1}{2}}R(\eta\tilde{T}' + T)) = 0, \tag{11c}$$

$$-p + 2S^{-\frac{1}{2}}(u_r - \mathrm{i}\alpha\bar{w}'\eta) - AS^{-1}R(T + \eta\tilde{T}') - \chi(\mathrm{i}\alpha\eta S^{-1}R) + \eta(1 - S^{-1}R\tilde{T})(\alpha^2 + A^2(m^2 - 1)) = 0, \tag{11d}$$

$$T_r + BT + \eta(\tilde{T}'' + B\tilde{T}') + \mathrm{i}\alpha\eta = 0, \tag{11e}$$

and the boundary conditions at $r = \beta$ are

$$u = v = w = T_r = 0, \tag{11f}$$

and where two approximations are possible:

$\chi = 0$ corresponds to the formulation used in Xu & Davis (1985); (12*a*)

$\chi = 1$ corresponds to the formulation used in Smith & Davis (1983). (12*b*)

5. Results

The two-point eigenvalue problem defined by (10), (11) is solved numerically by a combination of two methods. A starting algorithm is used to calculate one eigensolution at a branch. This algorithm combines a two-dimensional search for roots with a boundary-value solver and is described in detail in Dijkstra (1989). A spline interpolation of this numerically calculated solution provides the exact solution for the AUTO (Doedel 1980) software. With this software, continuation of eigenvalue branches can be performed in parameter space. In addition it is possible to continue limit points (folds) in parameter space. The prescribed accuracy in AUTO is $|\Delta \boldsymbol{u}|_\infty/(1 + |\boldsymbol{u}|_\infty) < \epsilon$ and $|\Delta\theta|/(1 + |\theta|) < \epsilon$ where $\boldsymbol{u}$ and θ indicate the solution vector and any (free) parameter, respectively. In a limit point continuation, $\epsilon = 10^{-4}$ is prescribed; in any other case $\epsilon = 10^{-6}$ is prescribed.

To justify the numerical results we compared them with analytic results obtained for axisymmetric long waves ($\alpha \to 0$), and with other available numerical results, i.e. the full cylinder (Xu & Davis 1985) and the two-dimensional layer ($A \to 0$) (Smith & Davis 1983). Our results ($\chi = 1$) are within 0.1 % of the values listed in table 1 of Smith & Davis ($\chi = 1$). To give an idea of the difference between the $\chi = 0$ and $\chi = 1$ approximations we note that our results for $\chi = 0$ are within 5% of the $\chi = 1$ values. Our numerical results compare favourably with analytic and other numerical results in all cases tested including comparisons with results of Russo & Steen (1989).

From now on, we only consider the base state $\mathscr{B}_1$, i.e. $Q = 0$ in (5) since it is more easily (physically) realizable than the base state $\mathscr{B}_0$.

5.1. *Base states subject to uniform ambient pressure: the one-parameter family.*

We recall from Russo & Steen (1989) that in the isothermal case and for $S = 10^4$, the region of complete stabilization of the axisymmetric $m = 0$ mode occurs at relatively small A. Therefore, we start with parameter values $A = 0.3$, $S = 10^4$, $B = 1$ and $P = 0.1$. In addition, we first consider $\chi = 0$. In figure 2, three eigenvalue branches are

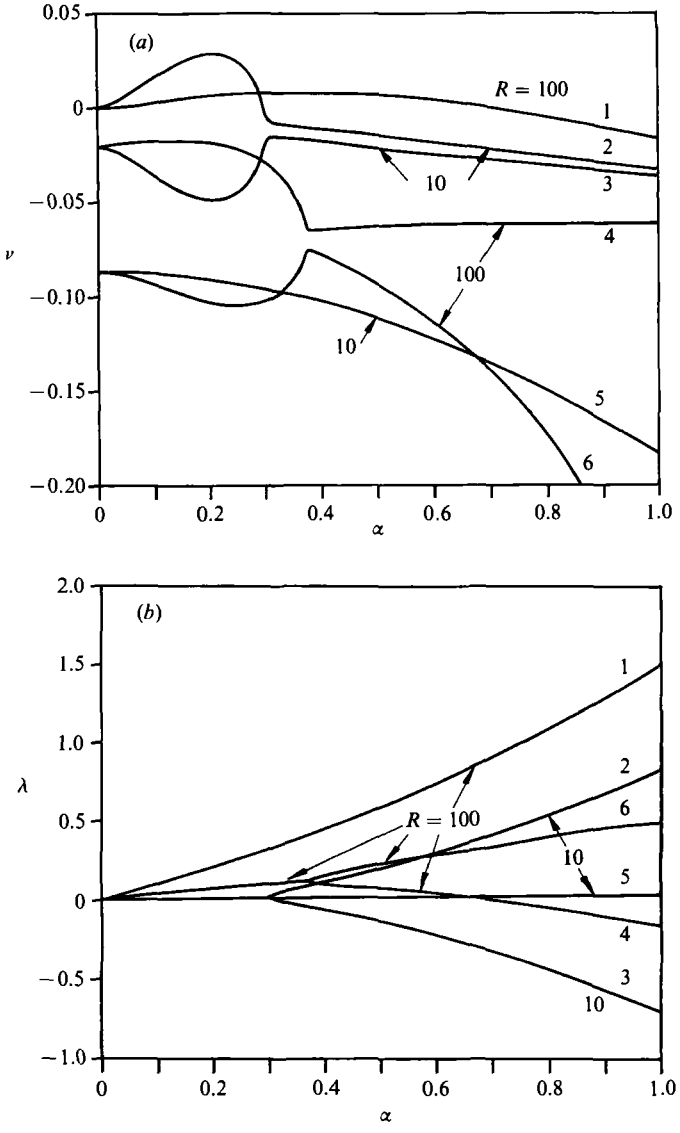

FIGURE 2. Eigenvalue branches for the axisymmetric ($m = 0$) mode showing (a) the growth factor ν and (b) the angular frequency λ as a function of the wavenumber α for values of the Reynolds number $R = 10$ and 100; the other parameters have values $B = 1$, $A = 0.3$, $P = 0.1$ and $S = 10^4$ (one-parameter family of base states ($\mathscr{B}_1$)). Curves in both figures belonging to the same eigenvalue branch have a common number.

shown, each for $R = 10$ and 100; the growth factor ν is shown in figure 2(a) and the angular frequency λ is presented in figure 2(b). Each eigenvalue branch (with eigenvalue $\lambda + i\nu$) is represented by one curve in each figure having a common number.

There are two branches which are unstable in a wavenumber interval (one for $R = 10$, one for $R = 100$). We observe that increasing R stabilizes long waves (capillary instabilities) but that large wavenumbers (shear waves) are destabilized. The unstable waves are travelling to the right (frequency is positive).

The neutral curves (locus of points (R, α) where the growth factor is zero) are

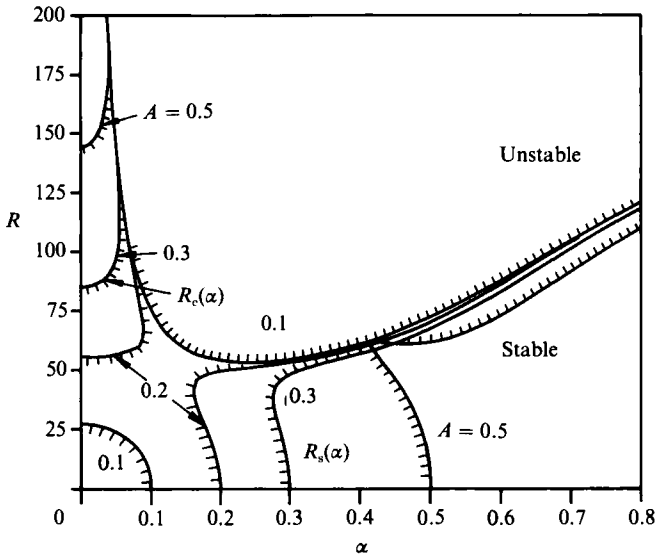

FIGURE 3. Neutral curves for the axisymmetric ($m = 0$) mode for different A and $B = 1, P = 0.1$ and $S = 10^4$ (one-parameter family of base states ($\mathscr{B}_1$)). Hatching along one side of a curve indicates the unstable region.

presented in figure 3 for several values of A and for the same values of χ, P, B and S. The neutral states for each A are comprised of two curves. Of the two branches only one exists for small wavenumbers. Let us call this the capillary branch $R = R_c(\alpha)$; the other branch we call the shear branch $R = R_s(\alpha)$. Each neutral curve divides the (α, R)-plane into a stable and unstable region. The unstable region is indicated by the hatches along each neutral curve.

As in the isothermal case, a window of shear stresses exists (for small A) at which complete stabilization to axisymmetric disturbances occurs. Note that the stabilization range appears through a topological change of the neutral curves. This transition occurs at sufficiently large α to have physical content with respect to restriction (9).

We now turn to the non-axisymmetric modes. Neutral curves for the $m = 0$, 1 and 2 modes are presented in figure 4 for $A = 0.1$. The other azimuthal modes, $m \geqslant 3$, are more stable than the $m = 2$ mode and are not shown. From this figure we conclude that the non-axisymmetric modes do not change the R-range for which complete stabilization occurs at $A = 0.1$. The minima of the $m = 0$, $m = 1$ and $m = 2$ neutral curves in this case (for $\alpha/A > 1$) are at $R = 53.0$, $R = 53.4$ and $R = 55.8$, respectively. Hence the $m = 1$ mode is only slightly more stable than the $m = 0$ mode at large wavenumbers. Note that for small wavenumbers the $m = 2$ mode is more unstable than the $m = 1$ mode.

Next, the effect of changing χ, S, P, B on the two boundaries of the R-interval for which complete stabilization occurs at $A = 0.1$ is considered. For this purpose, define $R_l = \max R_c(\alpha)$ and $R_u = \min R_s(\alpha)$. In addition, let α_l and α_u be the values of α for which these extrema are attained. In the case $\alpha_l = 0$ (we did not find a case for which $\alpha_l \neq 0$), R_l is calculated analytically by the long-wavelength analysis and its change in parameter space is obtained easily. The variation of (α_u, R_u) is obtained by a limit point (the minimum of the neutral curve) continuation, which is easily done with the AUTO software.

First the effect of taking $\chi = 1$ instead of $\chi = 0$ is determined. For $m = 0$, $A = 0.1$,

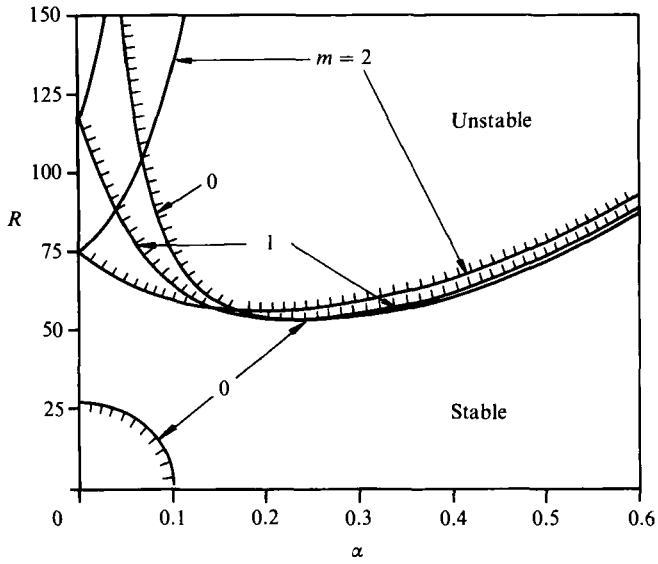

FIGURE 4. Neutral curves for the axisymmetric mode $m = 0$ and the non-axisymmetric modes $m = 1$ and $m = 2$ at $A = 0.1$, $B = 1$, $P = 0.1$ and $S = 10^4$ (one-parameter family of base states ($\mathscr{B}_1$)).

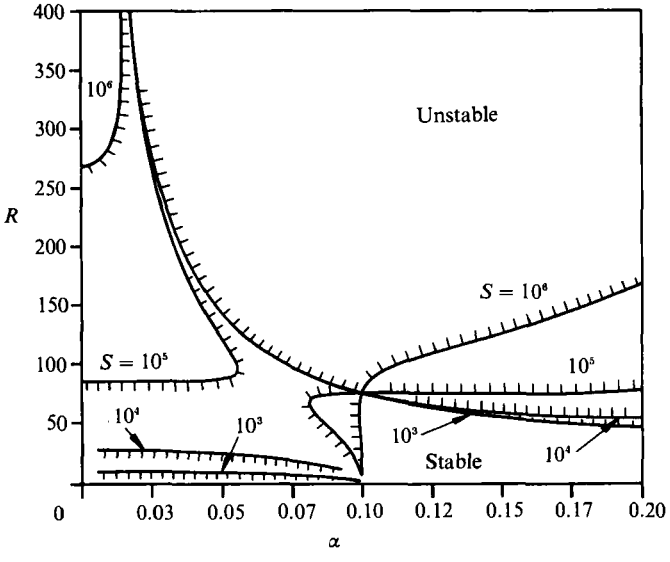

FIGURE 5. Neutral curves at different S for the axisymmetric ($m = 0$) modes with $P = 0.1$, $B = 1$ and $A = 0.1$ (one-parameter family of base states ($\mathscr{B}_1$)).

$S = 10^4$, $B = 1$, $P = 0.1$ and $\chi = 0$, the values of R_l and R_u are 26.8 and 52.9, respectively. For $\chi = 1$ these values change to 26.8 and 55.1, respectively. That χ does not influence R_l is clear from the equations since it is multiplied by α. Since the effect of χ on R_u is small, we shall use the value $\chi = 0$ from now on; taking $\chi = 1$ rather than $\chi = 0$ will not qualitatively change the picture of the neutral curves.

In figures 5 and 6, the effect of secondary parameters is shown. Neutral curves for selected values of S are shown in figure 5. Between $S = 10^4$ and $S = 10^5$ there is a topological change in the neutral curves, similar to that in figure 3. The values of R_l and R_u are shown as functions of S, B and P in figures 6(a), 6(b) and 6(c),

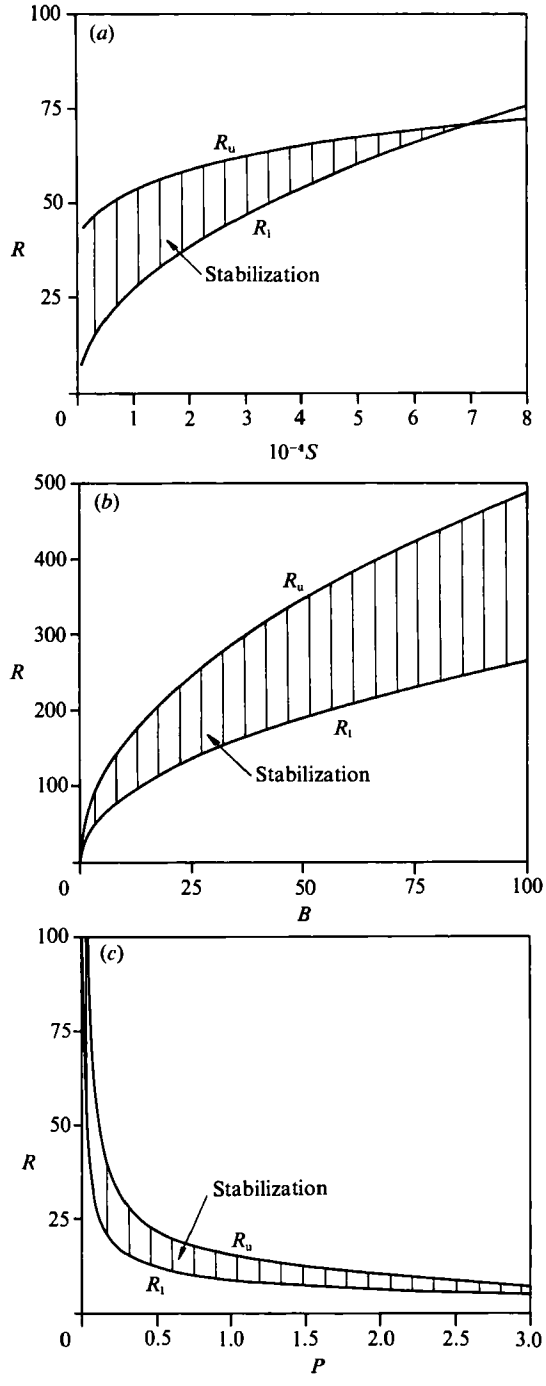

FIGURE 6. Effect of the secondary parameters S, B and P on the region of complete stability of the axisymmetric ($m = 0$) modes at $A = 0.1$ (one-parameter family of base states ($\mathscr{B}_1$)). The shaded area in (*a*) shows the dependence of the region on S for $P = 0.1$ and $B = 1$; (*b*) shows the dependence on B for $P = 0.1$ and $S = 10^4$; (*c*) shows the dependence on P for $B = 1$ and $S = 10^4$.

P	B	R_u	α_u
0	0.1	422.97	0.977
0	1	421.30	0.824
0	10	416.36	0.693
0	10^3	415.30	0.678
0.1	10^3	415.16	0.678
10	10^3	409.26	0.681
100	10^3	365.80	0.750

TABLE 1. Values of R_u and α_u for several P and B. The other parameter values are $A = 0.1$, $S = 10^4$, $m = 0$ and $M = 0$.

respectively. In each part of figure 6, the hatched region indicates the window in R for which complete stabilization occurs. For S larger than about 7×10^4 this window has disappeared. The window of stabilization increases with B; no topological changes in the neutral curves are found. A topological change similar to that in figure 5 occurs at $P = 3.28$, where complete stabilization disappears, just outside the view of figure 6 (*c*).

In summary, the range (R_l, R_u) over which applied thermocapillary shear stresses stabilize capillary breakup increases with decreasing P, increases with increasing B and increases with decreasing S. The qualitative picture of the neutral curve does not change with B. It can change on varying the other parameters, but there are only two topologically different possibilities. One of these implies a possible range of R (i.e. if $R_l < R_u$) for which complete stabilization exists (the picture for small P, small S and small A). The other implies no complete stabilization, since long waves are always unstable.

5.2. *Base states subject to a gradient in ambient pressure: the two-parameter family*

As explained above, a two-parameter family of base states is obtained by considering the base-state axial pressure gradient δ as a free parameter. Following Russo & Steen (1989), we use instead of δ the parameter

$$M \equiv \bar{w}'(\beta) \tag{13a}$$

and it follows readily that

$$M = \frac{\frac{1}{2}S^{\frac{1}{2}}}{(1-A)}\left(\delta(A-2)+\frac{2R}{S}\right). \tag{13b}$$

A negative value of M implies that $\bar{w}(r)$ has at least one zero on (β, γ), and hence the base state has a return-flow character. For slender bridges, it is expected that the 'return-flow' solutions corresponding to no net flow through each cross-section are a reasonable approximation to flows obtained in experiments with distant endwalls (boundaries in the z-direction).

First we put $S = 10^4$, $M = 0$, $m = 0$ and $A = 0.1$. The isothermal results can be obtained in the limits $B \to \infty$, $P \to 0$. Note that $B \to \infty$ alone does not decouple the flow field and thermal field as in Xu & Davis (1985) because $\tilde{T}'(\gamma)$ is in general non-zero. Taking $P = 0$ and $B = 10^3$, the isothermal results are indeed obtained up to 0.1%, which is an extra check on the numerical techniques used.

In table 1, the values of R_u and α_u are given for different P at $B = 10^3$ (monitoring the influence of non-zero $\tilde{T}'(\gamma)$, with disturbance interfacial temperature $T(\gamma) \approx 0$) and for different B at $P = 0$ (monitoring the influence of non-zero $T(\gamma)$, having

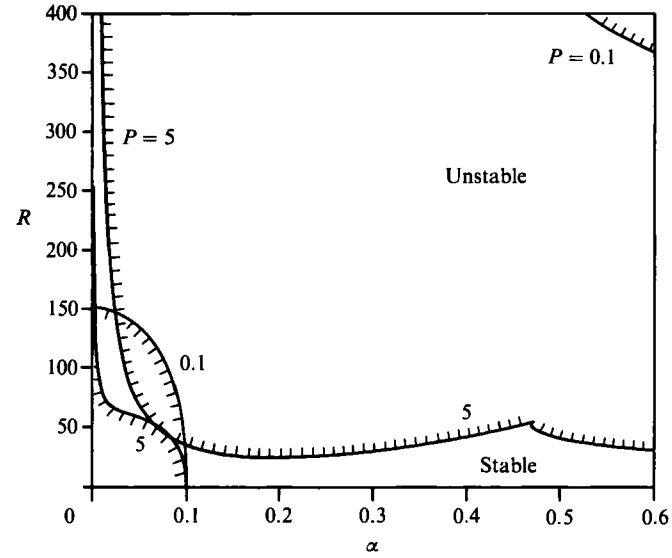

FIGURE 7. Neutral curves of the axisymmetric ($m = 0$) mode for $M = 0$, $B = 1$ $A = 0.1$ and $S = 10^4$ are presented for $P = 0.1$ and $P = 5$ (two-parameter family of base states ($\mathscr{B}_1$)).

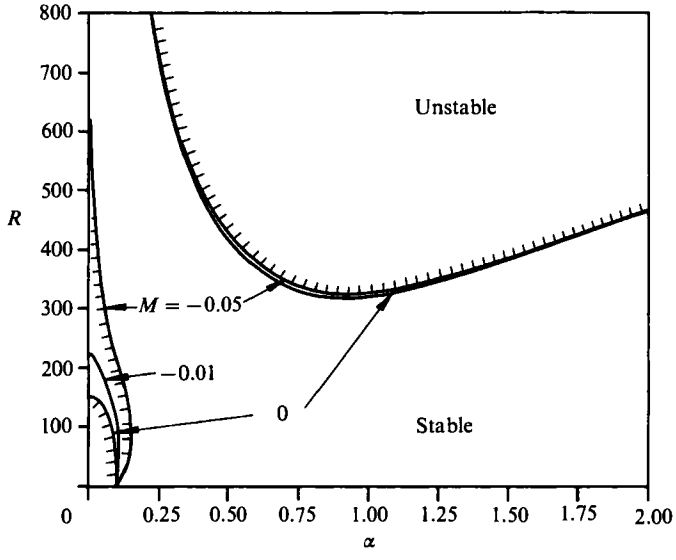

FIGURE 8. Neutral curves of the axisymmetric ($m = 0$) mode are shown for three values of M, with $S = 10^4$, $B = 1$, $P = 0.1$ and $A = 0.1$ (two-parameter family of base states ($\mathscr{B}_1$)).

$\tilde{T}'(\gamma) = 0$). The value of R_1 depends only on the ratio P/B, as will be shown below, and is in each case equal to the isothermal value ($R_1 = 149.22$). We observe that by decreasing B, for $P = 0$, we can increase the range of stabilization $R_u - R_1$. Table 1 shows that the (isolated) influence of the thermal base state on the disturbance flow field is weak for P up to 10. The (isolated) influence of the thermal disturbances on the disturbance flow field is weak over the whole B-range.

However, the combined influence can have a large effect on the stabilization range as can be seen in figure 7. Here the neutral curves for $P = 0.1$, $B = 1$ and those for $P = 5$, $B = 1$ are presented for $A = 0.1$. Increasing P, for $B = 1$, destabilizes long

wavelengths and complete stabilization disappears. Notice that this transition is to a new qualitatively different picture, somewhat like the long-wave transition in A for the isothermal case (figure 9a in Russo & Steen 1989).

For $A = 0.1$, $P = 0.1$, $B = 1$ and $S = 10^4$ neutral curves are shown in figure 8 for $M = 0$, -0.01 and -0.05. The shear branch for $M = -0.01$ is not explicitly shown since it nearly coincides with the corresponding curve for $M = 0$. One can see that for small negative M complete stabilization disappears. This is similar to what was found in the isothermal case (Russo & Steen 1989). Long waves become unstable for base states with a slight return-flow character.

6. Perturbation analysis for axisymmetric long-wave disturbances

To study the mechanism of stabilization of long axisymmetric waves (as observed, for example, in Russo & Steen 1989 figure 9a and here in figure 7) we use a perturbation approach $\alpha \to 0$ as in Benjamin (1957) and Yih (1963). After putting $m = 0$ and $\omega = \alpha c$, the equations for the perturbation quantities become

$$\mathrm{i}\alpha(\bar{w}-c)\,u = S^{-\frac{1}{2}}\left(u_{rr}-\alpha^2 u+\frac{u_r}{r}-\frac{u}{r^2}\right)-p_r, \tag{14a}$$

$$\bar{w}'u+\mathrm{i}\alpha(\bar{w}-c)\,w = S^{-\frac{1}{2}}\left(w_{rr}-\alpha^2 w+\frac{w_r}{r}\right)-\mathrm{i}\alpha p, \tag{14b}$$

$$P(\mathrm{i}\alpha(\bar{w}-c)\,T+\tilde{T}'u-w) = S^{-\frac{1}{2}}\left(T_{rr}+\frac{T_r}{r}-\alpha^2 T\right), \tag{14c}$$

$$u_r+\frac{u}{r}+\mathrm{i}\alpha w = 0, \tag{14d}$$

with boundary conditions

$$r=\beta: \qquad u = w = T_r = 0, \tag{15a}$$

$$r=\gamma: \qquad u+\mathrm{i}\alpha\eta(c-\bar{w}) = 0, \tag{15b}$$

$$w_r+\mathrm{i}\alpha u+\eta\bar{w}'' = -\mathrm{i}\alpha(\eta\tilde{T}'+T)\,S^{-\frac{1}{2}}R \tag{15c}$$

$$-p+2S^{-\frac{1}{2}}(u_r-\mathrm{i}\alpha\eta\bar{w}')-\eta(A^2-\alpha^2) = S^{-1}R(A(T+\eta\tilde{T}')-\tilde{T}\eta(A^2-\alpha^2)), \tag{15d}$$

$$T_r+BT+(\tilde{T}''+B\tilde{T}')\,\eta+\mathrm{i}\alpha\eta = 0. \tag{15e}$$

Applying the perturbation expansions

$$c = c_0+\alpha c_1+\alpha^2 c_2+O(\alpha^3), \quad u = \alpha u_1+\alpha^2 u_2+O(\alpha^3),$$
$$w = w_0+\alpha w_1+\alpha^2 w_2+O(\alpha^3), \quad p = p_0+\alpha p_1+\alpha^2 p_2+O(\alpha^3),$$
$$\eta = \eta_0+\alpha\eta_1+\alpha^2\eta_2+O(\alpha^3), \quad T = T_0+\alpha T_1+\alpha^2 T_2+O(\alpha^3),$$

and using the normalization $\eta_0 = 1$, $\eta_j = 0$, $j = 1, 2, \ldots$, the perturbation equations are solved at each order of α. It turns out that c_0 is real and that c_1 is determined by the following problem for $w_1(r)$:

$$S^{-\frac{1}{2}}\left(w_{1,rr}+\frac{w_{1,r}}{r}\right) = \mathrm{i}(p_0+(\bar{w}-c_0)\,w_0-\mathrm{i}\bar{w}'u_1), \tag{16a}$$

$$w_1(\beta) = w_{1,r}(\gamma)+\mathrm{i}S^{-\frac{1}{2}}R(\tilde{T}'(\gamma)+T_0(\gamma)) = 0, \tag{16b}$$

$$c_1 = \frac{\mathrm{i}}{\gamma}\int_\beta^\gamma [-\mathrm{i}rw_1(r)]\,\mathrm{d}r, \tag{16c}$$

where $w_0(r) = -\gamma\bar{w}''(\gamma)\ln(r/\beta)$, $\mathrm{i}u_1(r) = \frac{1}{4}\gamma\bar{w}''(\gamma)(r-2r\ln(r/\beta)-\beta^2/r)$,

$$c_0 = \bar{w}(\gamma)+\mathrm{i}u_1(\gamma), \quad p_0 = -A^2+AS^{-1}R(A\tilde{T}(\gamma)-\tilde{T}'(\gamma)-T_0(\gamma)),$$

$$T_{0r}(r) = -PS^{\frac{1}{2}}\mathrm{i}u_1(r), \quad T_0(\gamma) = -\tilde{T}'(\gamma)-B^{-1}(T_{0r}(\gamma)+\tilde{T}''(\gamma)).$$

It is easy to see that u_1, w_1 and c_1 are imaginary; let $\kappa = \mathrm{Im}(c_1)$. Recalling that the time-dependence of a disturbance is $\exp(-\mathrm{i}\omega t) = \exp(-\mathrm{i}\alpha c_0 t+\alpha^2\kappa t+O(\alpha^3))$, perturbations are amplified if $\kappa > 0$, while if $\kappa < 0$, they decay. The value of R (implicitly in the base state) at the neutral curve ($\alpha \to 0$) is determined by solving $\kappa(R) = 0$ for R.

Defining $f_1(r) = S^{\frac{1}{2}}r(\bar{w}(r)-c_0)\,w_0(r)-\mathrm{i}\bar{w}'(r)\,u_1(r)+p_0)$ one can show that

$$\gamma\kappa = -S^{-\frac{1}{2}}R\phi\gamma\mathcal{Q}(\gamma)-\int_\beta^\gamma \mathcal{Q}(r)f_1(r)\,\mathrm{d}r. \tag{17}$$

Here $\mathcal{Q}(r) = \frac{1}{2}\gamma^2\ln(r/\beta)-\frac{1}{4}(r^2-\beta^2)$ and $\phi = (\tilde{T}'(\gamma)+T_0(\gamma))$. Furthermore, it is easy to show that $\mathcal{Q}(r)$ is a positive function on $[\beta,\gamma]$ having a maximum at $r = \gamma$.

Equation (17) is the basic tool for explaining the mechanism of the shear stabilization of capillary breakup, as we shall see below.

7. Mechanism of stabilization of axisymmetric long waves: isothermal case

Since the non-isothermal case is most easily understood as a modification of the isothermal analysis, and since the mechanism of stabilization in the isothermal case has not previously been discussed, we present that case in some detail. We use the results from the long-wave analysis above and note that in the isothermal case ($P = 0$, $B = \infty$), the value of ϕ is zero and the right-hand side of (16a) is split into two pieces, $\mathrm{i}(p_0+\not{p}(r))$, where the capillary pressure $p_0 = -A^2$ here, and where $\not{p}(r)$ is defined by

$$\not{p}(r) = (\bar{w}-c_0)\,w_0-\mathrm{i}\bar{w}'u_1. \tag{18}$$

Inspection of the expression of the general (velocity) base state, shows that it is linear in both $S^{-\frac{1}{2}}R$ and M. Therefore, we can write $\bar{w}(r) = S^{-\frac{1}{2}}R\bar{w}_R(r)+M\bar{w}_M(r)$, where the definitions of $\bar{w}_R$ and $\bar{w}_M$ follow immediately. Hence, we can write $\not{p}(r) = S^{-1}R^2p_{RR}(r)+S^{-\frac{1}{2}}RMp_{RM}(r)+M^2p_{MM}(r)$, because w_0 and u_1 are proportional to $\bar{w}''(\gamma)$ and where the definitions of p_{RR}, p_{RM} and p_{MM} also follow immediately. Substituting this into (17), we obtain

$$\kappa = -\frac{S^{\frac{1}{2}}}{\gamma}[H_0+S^{-1}H_{RR}R^2+S^{-\frac{1}{2}}H_{RM}RM+H_{MM}M^2], \tag{19}$$

where the coefficients $H_i = \int_\beta^\gamma p_i(r)\,\mathcal{Q}(r)\,r\,\mathrm{d}r$ depend only on A.

The function $\not{p}(r)$ (equation (18)) represents an inertial acceleration effect due to the interchange of momentum between the base state and the disturbances. This momentum transfer gives rise to a flow which may be imagined, alternatively, as being caused by a pressure distribution. Since the origin of this 'pressure distribution' is inertia, Smith (1989) calls the resulting function $\not{p}$ an 'inertial pressure'.

For the moment we restrict consideration to $M = 0$. Since H_0 is negative, in view of (19) it follows that *no stabilization can occur if*

$$H_{RR}(A) = \int_\beta^\gamma r\mathcal{Q}(r)\,p_{RR}(r)\,\mathrm{d}r \leqslant 0. \tag{20}$$

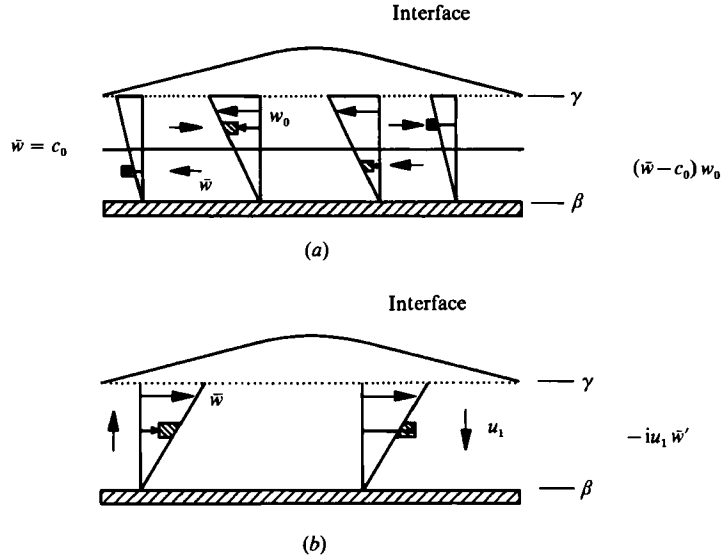

FIGURE 9. Sketch of the inertial acceleration effect due to the interaction of disturbances and base state. The axial acceleration (or deceleration) due to axial velocity disturbances (*a*), or due to normal velocity disturbances, (*b*), are represented by changes in velocities in the hatches regions.

The equality sign provides the value of A, say A_c, for which there exists no R to make κ negative, i.e. A_c is the boundary of shear stabilization of long waves. Through numerical evaluation of the integral, we obtain $A_c = 0.345478$, in accordance with the results of Russo & Steen (1989, figure 9*a*) where the neutral curves for all wavenumbers are calculated. For later discussion, we take this value to be the numerical definition of A_c.

In addition ($M = 0$ still), the positiveness of $\mathscr{D}(r)$ provides $S^{-1}R^2H_{RR}(A) \leqslant \frac{1}{2}(\gamma^2-\beta^2)\,\mathscr{D}(\gamma)\,\tilde{P}$, where $\tilde{P}$ is the area-averaged inertial pressure

$$\tilde{P} = 2(\gamma^2-\beta^2)^{-1}\int_\beta^\gamma r\,\mathscr{P}(r)\,\mathrm{d}r. \tag{21}$$

Hence if $\tilde{P} \leqslant 0$, no stabilization can occur. It turns out that $\tilde{P} = 0$ provides an upper bound for A_c. We obtain $A = 0.368411$ which has a relative error of about 7 %. This upper bound supports the suggestion made by Smith (1989) that the average inertial pressure may be a good indicator for the stability of the system to long waves.

7.1. *Physical mechanism of stabilization: $M = 0$*

In the description below of the mechanism of the stabilization of capillary breakup for the case $M = 0$, we follow closely the method of Smith (1990), although he considers a planar two-dimensional problem and explains a classical instability. The normalization for η used means that the free-surface deformation has the form of a cosine wave; $\eta = \exp(\mathrm{Im}\,(c)\,\alpha t)\cos\{\alpha(z-(\mathrm{Re}\,(c))\,t\}$; this is the disturbance applied to the system. Consider for the moment only that part of the interface corresponding to a surface elevation (cf. figure 9).

The leading-order effect of the elevation is a pressure decrease that is proportional to the interface deflection, initiating the usual capillary instability. Another effect is the appearance of a (disturbance) shear stress, at the interface equal to $-\bar{w}''(\gamma)\,\eta$. This shear stress drives an axial velocity perturbation w_0. This is the initiating mechanism of the shear instability. Hereafter a 'growth stage' starts.

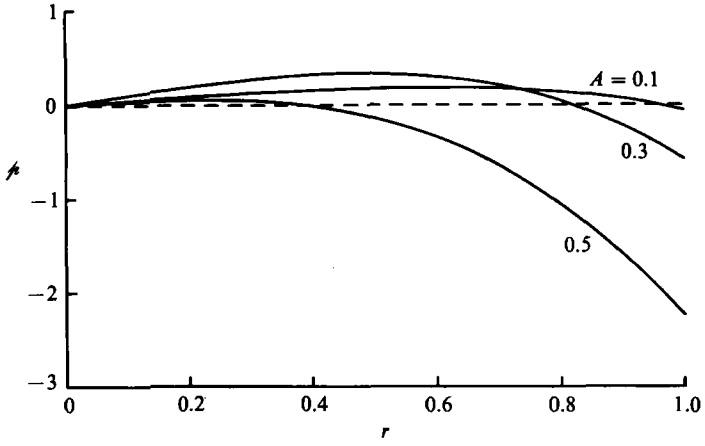

FIGURE 10. Radial dependence of the inertial pressure $\not{p}(r)$ for the isothermal case with $R = 522.63$, $M = 0$, $S = 10^4$: (*a*) $A = 0.1$, $c_0 = 7.75 \times 10^{-2}$, $\kappa = -3.76$, $\tilde{P} = 1.13 \times 10^{-1}$; (*b*) $A = 0.3$, $c_0 = 1.53 \times 10^{-1}$, $\kappa = -1.53 \times 10^{-3}$, $\tilde{P} = 1.18 \times 10^{-1}$; (*c*) $A = 0.5$, $c_0 = 4.00 \times 10^{-1}$, $\kappa = 3.61 \times 10^{1}$, $\tilde{P} = -5.84 \times 10^{-1}$.

In figure 9(*a*), consider the acceleration of the fluid particles due to the interaction of the base state and the axial disturbance (in the frame of the wave). Let r^* denote the point where $\bar{w} = c_0$ (note that this point might not exist on $[\beta, \gamma]$, for all A). Then on $[\beta, r^*]$ the fluid particles are accelerated from the bump, giving an effective stabilization. One can see this by looking at the right side of the bump, for example. Here the base state $(\bar{w} - c_0)$ convects the disturbance w_0 into an area where the disturbance velocities are larger. This effectively decreases the motion of the disturbance to the left. In the same way on $[r^*, \gamma]$ the fluid particles are accelerated towards the bump which destabilizes the system.

The normal velocity u_1 is out of phase with the interface deformation and is downwards on the right half of the bump and upwards on the left half of the bump. The interaction between the disturbances and the base state leads to a flow from the bump and is therefore stabilizing. Consider, for example, the right side of the bump in figure 9(*b*). The normal velocity perturbation u_1 moves fluid particles into a region where the base-state velocity is smaller ($\bar{w}' < 0$), effectively accelerating these particles to the right. Hence, there is movement from the bump.

In figure 10, the inertial pressure $\not{p}(r)$ (equal to $S^{-1}R^2 p_{RR}(r)$ for $M = 0$) is plotted as a function of r for $A = 0.1$, 0.3 and 0.5. Here $R = 522.63$, which is the value at the neutral curve for $A = 0.3$, $\alpha \to 0$ and $S = 10^4$. For $A = 0.1$ the base state is stable, while for $A = 0.5$ it is unstable. We observe that, as A decreases, the range of the function $\not{p}$ becomes more positive. This fact and relation (19) suggest a direct connection between the range of $\not{p}$ and the stability of the base state. Now $\not{p}$ is the sum of $(\bar{w} - c_0) w_0$ and $-\mathrm{i} u_1 \bar{w}'$ and the values of c_0 are shown in the caption. Because c_0 is positive in each case, the function $\bar{w} - c_0$ has a zero in (β, γ) and because the function w_0 is negative for each A the product $(\bar{w} - c_0) w_0$ also has one zero in (β, γ). The function $-\mathrm{i} u_1 \bar{w}'$ is a positive function. Clearly, for larger gap ratios the destabilizing capillary pressure along with shear effects swamps the stabilizing effects of shear.

The relative magnitude of the destabilizing and stabilizing effects which arise from the inertial acceleration determine whether or not capillary breakup is stabilized. The competition between these effects is determined by the function $\not{p}(r)$. A stabilizing effect is represented by a positive contribution to $\not{p}$. The interval where

A	H_0	H_{RR}	H_{RM}	H_{MM}
0.1	-3.34×10^{-2}	1.50×10^{-2}	1.32	-1.33
0.3	-1.02×10^{-1}	3.73×10^{-3}	4.58×10^{-1}	-4.34×10^{-1}
0.5	-1.78×10^{-1}	-1.99×10^{-2}	3.20×10^{-1}	-2.43×10^{-1}
0.7	-2.77×10^{-1}	-9.46×10^{-2}	3.13×10^{-1}	-1.44×10^{-1}
0.9	-4.82×10^{-1}	-6.40×10^{-1}	3.98×10^{-1}	-5.36×10^{-2}

TABLE 2. Values of the coefficients H as a function of the gap ratio A

A_d	M_d	$S^{-\frac{1}{2}}R_d$
0.35	3.56×10^{-2}	1.68×10^{1}
0.50	4.13×10^{-1}	3.31
0.65	1.13	2.65
0.80	3.06	2.46
0.95	1.71×10^{1}	2.35

TABLE 3. Values of $(M_d, S^{-\frac{1}{2}}R_d)$ as a function of A_d for the isothermal case. For $A_d < A_c$ there does not exist such a type of transition.

$\not{p}$ is positive accounts for the positive pressure buildup in the interior of the layer, causing a net flow from the bump. As can be seen from figure 10, this interval gets bigger as A decreases and disappears with increasing A. The competition determines the net result of the growth stage. A slightly different view of this stabilization mechanism has been presented in Russo (1990).

For $A \to 0$, long waves are stable for $M = 0$ in the isothermal case (Smith & Davis 1982). In terms of the above mechanism, as the gap ratio gets smaller, the wave speed $c_0 \to 0$ and the stabilizing influence of the axial perturbation velocity w_0 decreases while the stabilizing influence of the normal velocity perturbation u_1 increases. Taken in combination these two effects are always sufficiently stabilizing to beat the weakening destabilization of the capillary pressure ($p_0 = -A^2$) as $A \to 0$.

7.2. *Results and mechanism*: $M \neq 0$

We now turn to $M \neq 0$ and ask whether stabilization of long waves can occur. In table 2, the values of the coefficients H as a function of A are presented. Observe that only H_{RR} changes sign (at A_c) and that $H_{RM}^2 - 4H_{RR}H_{MM}$ is always positive. Immediately from this table and (19) the following result is obtained: there can be no stabilization if

$$D = M^2(H_{RM}^2 - 4H_{RR}H_{MM}) - 4H_{RR}H_0 < 0. \tag{22}$$

If $D > 0$, there are two possible situations for which stabilization to long waves can occur, depending on the number of real roots of the quadratic in R. In the first case ($H_{RR}^{-1}(H_0 + M^2H_{MM}) < 0$ and $MH_{RM}/H_{RR} \leqslant 0$), long waves are stable for $R > R_1$ and unstable for $R < R_1$. In the second case ($H_{RR}^{-1}(H_0 + M^2H_{MM}) > 0$ and $MH_{RM}/H_{RR} < 0$), there is an interval (R_2, R_3) for which long waves are stable. Since H_0 and H_{MM} are negative functions of A, the first case occurs for $A < A_c$ and only if $M \leqslant 0$. The second case occurs for $A > A_c$ and only if $M > 0$.

In the second case, there may exist a transition at some M_d where the interval (R_2, R_3) shrinks to one point at M_d and stabilization disappears for M passing through M_d. This does indeed occur, and values of the critical point $(M_d, S^{-\frac{1}{2}}R_d)$ are presented in table 3 as a function of A (which is indicated as A_d). An example of this singularity occurs in figure 11 (*b*) in Russo & Steen (1989) near the $A_d = 0.5$ ($S = 10^4$) value.

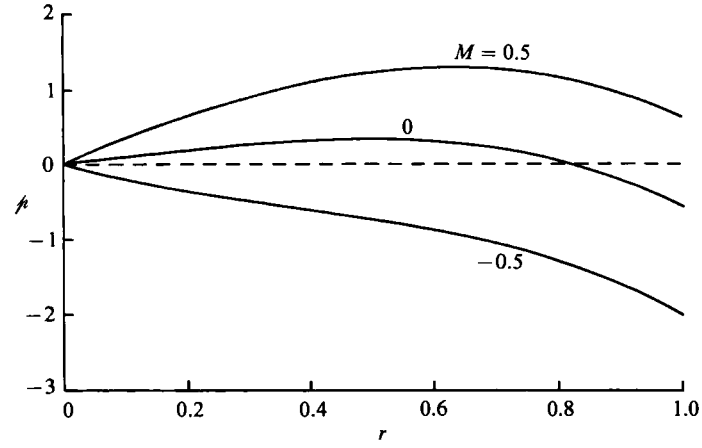

FIGURE 11. Change of inertial pressure distribution $\hat{p}(r)$ for $M = -0.5$, 0 and 0.5, at $R = 522.63$, $S = 10^4$ and $A = 0.3$. This illustrates the isothermal transition to stable long waves as M is increased at $A = 0.3$: (*a*) $M = -0.5$, $c_0 = -3.12 \times 10^{-1}$, $\kappa = 3.92 \times 10^1$, $\tilde{P} = -8.76 \times 10^{-1}$; (*b*) $M = 0$, $c_0 = 1.53 \times 10^{-1}$, $\kappa = -1.53 \times 10^{-3}$, $\tilde{P} = 1.18 \times 10^{-1}$; (*c*) $M = 0.5$, $c_0 = 6.18 \times 10^{-1}$, $\kappa = -3.27 \times 10^1$, $\tilde{P} = 9.46 \times 10^{-1}$.

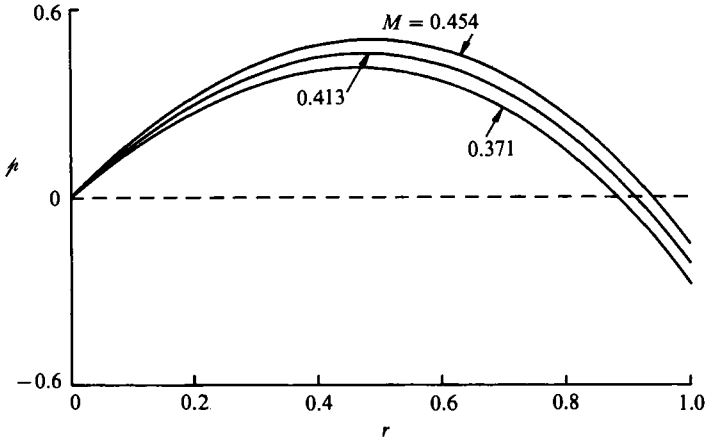

FIGURE 12. Change of inertial pressure distribution $\hat{p}(r)$ with varying M, at $R = 331.42$, $S = 10^4$, $A = 0.5$. This shows the isothermal transition at $M = M_d$ to stable long waves as M is increased: (*a*) $M = 3.71 \times 10^{-1}$, $c_0 = 3.41 \times 10^{-1}$, $\kappa = 1.80$, $\tilde{P} = 2.14 \times 10^{-1}$; (*b*) $M = 4.13 \times 10^{-1}$, $c_0 = 3.76 \times 10^{-1}$, $\kappa = -4.46 \times 10^{-5}$, $\tilde{P} = 2.59 \times 10^{-1}$; (*c*) $M = 4.54 \times 10^{-1}$, $c_0 = 4.11 \times 10^{-1}$, $\kappa = -1.75$, $\tilde{P} = 3.03 \times 10^{-1}$.

Going back to the physics, we focus on two transitions where long waves are stabilized. For both transitions we compute the inertial pressure $\hat{p}(r)$ and the area-averaged inertial pressure $\tilde{P}$. First, for $A = 0.3$, $S = 10^4$ and for $R = 522.63$ we present $\hat{p}(r)$ for $M = -0.5$, 0 and 0.5 in figure 11. As M is increased the range of the function $\hat{p}$ is becoming more positive, leading to stabilization. Also $\tilde{P}$ suggests a transition may occur since it changes sign between $M = -0.5$ and $M = 0$ (see figure caption).

Second, we fix $R = 331.42$, $S = 10^4$ and $A = 0.5$ and show this pressure distribution for $M = 0.371$, 0.413 and 0.454 in figure 12. Note from table 3 that at ($M_d = 0.413$, $S^{-\frac{1}{2}}R_d = 3.31$) there is a transition of the second type discussed above. The M-interval is chosen as $[0.9M_d, 1.1M_d]$. The quantity $\tilde{P}$ remains positive on this interval and hence in this case gives no indication of a transition. This emphasizes that a change in $\tilde{P}$ is not necessary for a change in stability.

For both transitions (figures 11 and 12) the inertial acceleration effect due to the interaction of the base state and the disturbances causes the stabilization. Therefore the above-sketched mechanism ($M = 0$) also applies to the case of $M \neq 0$. The main reason why a base state with a slight return flow is unstable to long waves is the fact that the phase speed c_0 becomes negative quickly for small negative M. This enhances the destabilizing effect of the inertial acceleration due to the presence of the axial velocity disturbance (as sketched in figure 9a).

8. Mechanism of axisymmetric long-wave stabilization: thermocapillary case

In contrast to the isothermal case, the physical significance of the thermocapillary solutions for $\alpha \to 0$ is brought into question by restriction (9). Strictly speaking, restriction (9) is always violated in the long-wave limit. However, as illustrated in the previous section with regard to the isothermal flow, transitions which occur at finite wavenumber can often be brought into the long-wave regime by adjustment of the other parameters. Hence, as long as the transitions we study in the long-wave limit are robust, the understanding gained will be useful when the transitions are perturbed to occur at finite wavelengths where restriction (9) can be satisfied.

Applying the same decomposition of the general base-state velocity profile as in the previous section we obtain from (17)

$$\kappa = -\frac{S^{\frac{1}{2}}}{\gamma}[G_0 + S^{-1}G_{RR}R^2 + S^{-\frac{1}{2}}G_{RM}RM + G_{MM}M^2], \tag{23}$$

where $G_0 = H_0$, $G_{RR} = H_{RR} + (P/B)F_{RR}$, $G_{RM} = H_{RM} + (P/B)F_{RM}$ and $G_{MM} = H_{MM}$. Here F_{RR} and F_{RM} depend only on the parameter A. From (16), we observe that the thermal field influences the long-wave stability in two ways. First, the base-state temperature and the disturbance temperature at the interface exert an influence through the normal stress balance since the magnitude of the surface tension depends on temperature. This effectively changes the first-order (capillary) pressure disturbance. Second, gradients of the temperature field influence the (Marangoni) tangential stresses at the interface. Both effects are incorporated in the coefficients F_{RR} and F_{RM}. For later reference, we need only split F_{RR} into terms which represent these effects. Let $F_{RR} = F_{\mathrm{n}RR} + F_{\mathrm{t}RR}$ where the subscripts n and t refer to the normal and tangential effects, respectively. The values of the coefficients $F_{\mathrm{n}RR}$, $F_{\mathrm{t}RR}$ and F_{RM} are presented in table 4. We refer to these values below.

Observe that for long waves, the disturbances depend on P and B only through P/B which can be seen from the disturbance equations, since for $\alpha = 0$, the thermal boundary condition decouples from the other equations. As in the isothermal case, we split the discussion of the thermocapillary case into three parts. First we consider the one-parameter family of base states; thereafter we discuss the two-parameter family cases, $M = 0$ and then $M \neq 0$.

8.1. *One-parameter family of base states*

In this case, M is not an independent parameter, since $M = S^{-\frac{1}{2}}Rg(A)$, where $g(A) = (A^2 - 2A + 2)/(2(1-A))$. Substituting this in (23) we obtain

$$\kappa = -\frac{S^{\frac{1}{2}}}{\gamma}[G_0 + S^{-1}(G_{RR} + G_{RM}g(A) + G_{MM}g^2(A))R^2]. \tag{24}$$

A	F_{tRR}	F_{nRR}	F_{RM}
0.1	-9.48×10^{-3}	6.17×10^{-3}	4.61
0.3	-3.84×10^{-2}	2.38×10^{-2}	1.34
0.5	-9.39×10^{-2}	5.51×10^{-2}	7.12×10^{-1}
0.7	-2.25×10^{-1}	1.25×10^{-1}	4.53×10^{-1}
0.9	-7.71×10^{-1}	4.02×10^{-1}	2.71×10^{-1}

TABLE 4. Values of the coefficients F as a function of A

A	$(P/B)_c$
0.05	1.12×10^{1}
0.10	4.53
0.15	2.34
0.20	1.27
0.25	6.55×10^{-1}
0.30	2.56×10^{-1}

TABLE 5. Values of the critical value $(P/B)_c$ at which long waves become unstable for every R. Note that such a transition does not exist for $A > A_c$.

A_d	M_d	$S^{-\frac{1}{3}}R_d$
0.1	-5.94	1.51×10^{3}
0.3	1.79	1.47×10^{2}
0.5	1.00	8.82
0.7	6.89×10^{-1}	1.35
0.9	4.80×10^{-1}	1.59×10^{-1}

TABLE 6. Values of M_d and $S^{-\frac{1}{3}}R_d$ for the thermocapillary case, $P/B = 1$, as a function of A_d

It turns out that the coefficient of R^2 is always positive, which implies that there is always one positive R for which $\kappa = 0$. This is in agreement with the numerical results presented in §5.

8.2. *Two-parameter family of base states: transition in P for M = 0*

The growth rate κ is given by (23) with $M = 0$. We again have the immediate result that long waves are unstable if $G_{RR} \leqslant 0$ with equality sign at the point $(A, (P/B)_c)$. This explains the long-wave transition in P observed in figure 7; the value of $(P/B)_c = -H_{RR}/F_{RR} = 4.53$ for $A = 0.1$. Furthermore, since the long-wave restriction is the limiting restriction for general wavenumber, it also characterizes the transition to complete stabilization (cf. figure 6*c*). The dependence of this transition value $(P/B)_c$ on A is indicated in table 5. Note that because F_{RR} is negative, this transition can only occur for $A < A_c (\equiv 0.345478)$. We now turn to the mechanism of long-wave stabilization due to thermocapillary-driven flow that corresponds to this transition. The stabilization occurs for decreasing P, for $M = 0$, $A = 0.1$ and $B = 1$ (figure 7).

The initiation stage is much like the one for the isothermal case. The only difference is the increase of p_0 (less negative) due to the dependence of surface tension on temperature (F_{nRR} is positive). During the growth stage, the inertial pressures are unchanged, relative to the isothermal case. Long waves become unstable with increasing P due to the added Marangoni shear stress. The surface tension disturbance along the interface is in phase with the interface deflection. Since F_{tRR} is negative, the disturbance surface tension is positive (disturbance temperature is

negative) at surface elevations. At depressions, just the opposite occurs. The net result is a flow from depressions to elevations which is destabilizing. For large enough P, this additional effect can destabilize long waves relative to the isothermal case.

8.3. *Two-parameter family of base states: transition in M, $M \neq 0$.*

Just as in the isothermal case, there can be transitions at an M_d where an R-interval for which long waves are stable disappears. Calculated values of M_d are presented in table 6. It is interesting that through the influence of the thermal field the values of M_d can be negative. This situation occurs at small A. Hence even return-flow base states can be stable to long waves for a certain range of applied shear.

9. Discussion

A linear stability analysis shows that an annular film of liquid put in axial motion by a thermocapillary-generated shear (one-parameter family of base states) or some combination of thermocapillary-generated shear and an axial pressure gradient (two-parameter family of base states) can be stable to disturbances of all wavelengths for motions of moderate Reynolds number. In the absence of motion, the interface succumbs to the capillary instability (long wave) and for strong enough motions it is susceptible to surface-wave instability (short wave). Some evidence (largely experimental) suggests that the surface-wave instability is less dangerous (in that it may saturate nonlinearly to finite amplitudes) than the capillary instability which inevitably leads to a loss of integrity of the liquid film (breakup). We focus on the inhibition of the 'stronger' instability, i.e. stabilization of the capillary instability.

In terms of the neutral curves R *vs.* α, complete stabilization appears as a window bounded above by the surface-wave neutral curve and below by the neutral curve corresponding to capillary instability. Results show that as control parameters are varied stabilization first occurs through a topological change in neutral curves. The gap ratio A is generally the parameter with the strongest influence. As A is decreased, for example, the (typical) topological change is described by a saddle-point singularity at finite wavelength in the neutral surface ((R, α, A)-space, e.g. figure 3). It appears that, locally, this singularity, which marks the birth of the window of stabilization, is described by a quadratic form in R and α. Its occurrence at finite α means that several terms, at least, must be calculated if it is to be accessible to a long-wave analysis and even then there is no guarantee. Indeed, depending on the character of the perturbation expansion, it may be inaccessible even with the calculation of an infinite number of terms. Rather than undertake such a lengthy (and risky) calculation, we exploit the presence of additional system parameters P, B and S (and M for the two-parameter family of base states) by adjusting their values to bring the 'birth' singularity to the long-wave limit. Appropriate adjustments of either S or P will do the job (figures 6*a* or 6*c*, respectively). In this way, the fully numerical calculations justify the long-wave analysis even though the long-wave analysis violates restriction (9). The numerical calculations also yield a limited optimization of the stabilization windows. These calculations show that stabilization is favoured by small A, small P, large B and relatively small S.

The long-wave analysis leads to a detailed understanding of the stabilization phenomenon. The axial velocity in the annulus, $\bar{w}$, interacts with the induced axial and radial perturbation velocities, w' and u', respectively, through the inertial terms, $\bar{w}w'_z$ and $\bar{w}_r u'$, to generate a disturbance 'pressure' field of opposite sign to the destabilizing pressure field due to the capillary disturbance. The strength of the

stabilizing 'pressure' field depends on the velocity profile and therefore is most strongly influenced by the parameters M and R. On the other hand, for a fixed profile (fixed R and M) the strength of the destabilizing pressure is controlled by the curvature of the base-state interface (i.e. by A): in particular, it vanishes as the mean interface radius becomes unbounded (as $A \to 0$).

This picture of the physical mechanism, drawn for the isothermal case, needs only slight modification to account for thermocapillary stabilization. Here, the applied shear stress τ in the definition of R is replaced by the thermocapillary-generated shear $\sigma_0 \zeta b$ and the additional parameters, Prandtl number P and Biot number B, influence the long-wave behaviour as P/B. In the simplest case, $M = 0$, increasing P/B increases the (mean) temperature at the interface and the imposed temperature gradient. This leads to competing influences on the disturbance growth rate. The enhanced surface temperature decreases the surface tension, weakening the capillary disturbance pressure (stabilizing), while the increased gradient increases the shear stress and thereby the growth rate (destabilizing). Over the range of gap ratios, the destabilizing effect is stronger (table 4) leading to an overall narrowing of the window of stabilization as compared to the isothermal case. When $M \neq 0$, there is an additional effect due to the influence of the thermal field on the disturbance velocity field, which is stabilizing for $M > 0$ and destabilizing if $M < 0$. This effect can dominate for $M = O(1)$ and A small.

Finally, the long-wave analysis leads to an explicit algebraic form for the neutral points (limit of the neutral curves as $\alpha \to 0$) in parameter space. This analytic equation verifies cases from the full numerical calculations (where the birth of stabilization has been observed to occur at $\alpha = 0$) and predicts other births not yet observed. Thus, despite its contradiction to the restriction (9), the long-wave analysis is useful for the thermocapillary study, not only to develop the mechanism of stabilization, but as a check on the numerical solution and as a guide to regions of interesting behaviour in the parameter space.

This work was partially supported by the US Army Research Office through the Mathematical Sciences Institute of Cornell University and partially supported by the National Aeronautics and Space Administration through NAG 3-801. This research was conducted using the Cornell National Supercomputer Facility, a resource of the Cornell Theory Center, which is funded in part by the National Science Foundation, New York State, the IBM Corporation and members of the Center's Corporate Research Institute.

REFERENCES

BENJAMIN, T. B. 1957 Wave formation in laminar flow down an inclined plane. *J. Fluid Mech.* **2**, 554–574.

CHARLES, M. E., GOVIER, G. W. & HODGSON, G. W. 1961 The horizontal pipeline flow of equal density oil-water mixtures. *Can. J. Chem. Engng* **39**, 17–36.

DIJKSTRA, H. A. 1989 The coupling of Marangoni and capillary instabilities in an annular thread of liquid. *J. Colloid Interface Sci.* **136**, 151–159.

DOEDEL E. J. 1980 AUTO: A program for the automatic bifurcation analysis of autonomous systems. In *Proc. 10th Manitoba Conf. on Numerical Maths and Comput.*, vol. 30, pp. 265–274.

MURPHY, S. P., HENDRICK, J. J., MARTIN, M. J., GRANT, R. W. & LIND, M. D. 1987 Floating zone processing of indium in earth-orbit. *Mat. Res. Soc. Symp. Proc.* **87**, 139–142.

PREZIOSI, L. G., CHEN, K. & JOSEPH, D. D. 1989 Lubricated pipelining: stability of core-annular flow. *J. Fluid Mech.* **201**, 323–356.

RUSSELL, T. W. F. & CHARLES, M. E. 1959. The effect of the less viscous liquid in the laminar flow of two immiscible liquids. *Can. J. Chem. Engng* **39**, 18–24.

RUSSO, M. J. 1990 Capillary instability and shear stabilization of liquid columns and bridges. Ph.D. dissertation, Cornell University.

RUSSO, M. J. & STEEN, P. H. 1989 Shear stabilization of the capillary breakup of a cylindrical interface. *Phys. Fluids* A **1**, 1926–1937.

SMITH, M. K. 1989 The axisymmetric longwave instability of a concentric two-phase pipe flow. *Phys. Fluids* A **1**, 494–506.

SMITH, M. K. 1990 The mechanism for the longwave instability in thin liquid films. *J. Fluid Mech.* **217**, 469–485.

SMITH, M. K. & DAVIS, S. H. 1982 The instability of sheared liquid layers. *J. Fluid Mech.* **121**, 187–206.

SMITH, M. K. & DAVIS, S. H. 1983 Instabilities of dynamic thermocapillary layers. Part 2. Surface-wave instabilities. *J. Fluid Mech.* **132**, 145–162.

XU, J. J. & DAVIS, S. H. 1985 Instability of capillary jets with thermocapillarity. *J. Fluid Mech.* **161**, 1–25.

YIH, C. S. 1963 Stability of liquid flow down an inclined plane. *Phys. Fluids* **6**, 321–334.

ZUBILLAGA, V., PATERNO, J., GUEVARA, E. & ROMERO, T. 1985 Pipelining of heavy crude oils using core annular flow. In *Proc. 3rd Intl Conf. on Heavy Crude and Tar Sands, New York, 22–31 July, 1985*. UNITAR/UNDP Information Centre, New York.